Accurate path-integral molecular dynamics calculation of aluminum with improved empirical ionic potentials

Zixiang Yan,[1] Chunyi Zhang,[2] Xing Liu,[3,1] Qing Miao,[4] Ming Fang,[4] and Wei Kang[2,*]
[1]*HEDPS, Center for Applied Physics and Technology and School of Physics, Peking University, Beijing 100871, China*
[2]*HEDPS, Center for Applied Physics and Technology and College of Engineering, Peking University, Beijing 100871, China*
[3]*China Institute of Nuclear Industry Strategy, Beijing 100048, China*
[4]*China Aerodynamics Research and Development Center, Mianyang 621000, China*

(Received 28 June 2022; revised 2 November 2022; accepted 7 November 2022; published 15 November 2022)

We show that an accurate description of the interplay between the anharmonic ionic interaction and the zero-point fluctuation of ions in crystalline aluminum (Al) can be achieved using the path-integral molecular dynamics (PIMD) method in conjunction with improved empirical modified embedded-atom method (MEAM) potentials. Our results show that the zero-point fluctuation of ions is noticeable at a temperature between 200 K and 250 K, roughly half of the Al Debye temperature of 428 K, with a selective influence on mechanical properties. The effect provides appreciable corrections to the lattice constant a, bulk modulus B, and elastic constant C_{11} at low temperature, but without much influence on elastic constants C_{12} and C_{44}. With a revised MEAM potential which takes into consideration the influence of zero-point fluctuations, the PIMD method has a much improved accuracy in a, B, and the C's up to 700 K, when compared with precision experimental measurements. The largest errors of a and B can even be reduced by about an order in percentage below 300 K.

DOI: 10.1103/PhysRevB.106.174107

I. INTRODUCTION

Thermal and mechanical properties of materials at very low temperature are of persisting interest to the exploration of outer space [1–3]. It is also found recently that they played a pivot role in cutting-edge scientific apparatuses such as inertial confined fusion devices [4], which may further boost corresponding investigations [5]. An improved description of materials' structure and their responses to external stresses at low temperature is thus an important topic of theoretical investigations of these fields. Preceding studies [6–11] have shown that the interplay between the anharmonic ionic interaction and the zero-point fluctuation of ionic motion [12] plays an important role in a series of unique properties at cryogenic temperature, e.g., bond-length increasing [6,7], decreasing of thermal expansion [8–10], and enhancement of heat capacity [11], which poses new challenges to microscopic methods, such as the molecular dynamics (MD) method [13], to provide a satisfactory description.

In the classical MD method, which is commonly used to describe ionic motion at a relatively high temperature, ions are viewed as classical particles, and their motions are described by Newton's law [13]. The highly anharmonic interaction between ions may be captured by an appropriately constructed interaction potential under this condition. However, at low temperature, when the quantum-mechanical feature of the system gradually takes dominance, the departure of ionic motion from the classical MD description becomes significant [14]. In previous works [15,16], the deviation of phonon distribution from Boltzmann distribution and the zero-point fluctuation of ionic motion, originated from Heisenberg's uncertainty principle, have been vigilantly noticed. A direct solution has been provided with the Feynman path-integral (PI) approach [12,17], where the description of ions as pointed particles is replaced by path loops.

But even with this improved methodology, one may still not be able to arrive at a satisfactory prediction to those properties closely associated with anharmonic interactions between ions, e.g., lattice constant and bulk modulus. The subtle issue here is the accuracy of ionic interaction, especially the highly anharmonic part which interplays with the zero-point fluctuation of ions at low temperature. In principle, an explicit quantum-mechanical description of the surrounding electrons would provide the most accurate ionic interaction, which may be achieved with the most advanced approximations so far to electrons' exchange and correlation interactions [18–20]. However, it is still a challenge for quantum-mechanical methods to provide predictions on thermal and mechanical properties that have comparable accuracy as in precise experimental measurements [21], and this approach may also incur huge computational costs [22] when dealing with real materials.

In practice, empirical ionic potentials, e.g., embedded-atom method (EAM) potentials [23–29], modified EAM (MEAM) potentials [30–35], and Tersoff-type potentials [36–38], are more commonly used when computational cost is a major concern. But those empirical potentials are generally parametrized for MD method at relatively high temperature. Their description of the anharmonic part is questionable at low temperature, when quantum effects of ions, especially the zero-point

*weikang@pku.edu.cn

fluctuations, are prominent. This may severely constrain the predictive capability of the calculation. It is thus of great interest, not only theoretically but also practically, if both the quantum effect of ions and their anharmonic interactions at relatively low temperature are well described simultaneously.

We show in this article, with aluminum (Al) as an illustrating example, that an accurate description of the interplay between the anharmonic ionic interaction and the zero-point fluctuation of ions can be achieved with the path-integral molecular dynamics (PIMD) method [39] in conjunction with improved empirical MEAM potentials. Al is chosen as the example for two reasons. One is that Al has been studied intensively as a typical metallic material [40–47], and the other is that there are high-precision experimental data available for Al [48–51]. With two MEAM potentials revised from the parametrization of Pascuet *et al.* [34] and Aitken *et al.* [35], a series of PIMD results of crystalline Al are presented at temperatures from 50 K to 700 K.

Our results show that the quantum zero-point fluctuation becomes noticeable at a temperature between 200 K and 250 K, roughly half of the Al Debye temperature of 428 K, suggesting that this effect is significant enough to be considered even at a relatively high temperature. In addition, it displays a selective influence on measured quantities. At low temperature, the effect provides an appreciable correction to the lattice constant a, bulk modulus B, and elastic constant C_{11}, but without much influence on elastic constants C_{12} and C_{44}. Furthermore, with the revised MEAM potentials taking the influence of zero-point fluctuations into consideration, the PIMD method has a much improved accuracy in the prediction to those properties associated with anharmonic interactions, compared with precision experimental results below 700 K. Especially, the largest errors of a and B are reduced by about an order in percentage below 300 K. In addition, the revision procedure of the MEAM potential provides a possible way to further improve the accuracy of low-temperature ionic potentials generated based on quantum-mechanical calculations by taking the correction from experimental measurements into consideration.

The rest of this article is organized as follows. A brief summary of the PIMD method and its computational details are presented in Sec. II. A concise description of the fitting procedure for the determination of MEAM parameters is provided in Sec. III. The main results of the lattice constant, bulk modulus, and elastic constants together with corresponding analyses are given in Sec. IV. A short summary is provided in Sec. V.

II. PATH-INTEGRAL MOLECULAR DYNAMICS METHOD

In the formulation of the PI method, the partition function of an N-particle system at temperature T is evaluated as the trace of the system's density matrix ρ, i.e., $Z \equiv \int d\boldsymbol{R}\rho(\boldsymbol{R},\boldsymbol{R};\beta)$, where $\beta = 1/k_BT$ is the inverse temperature (where k_B is the Boltzmann constant), and $\boldsymbol{R} \equiv \{\boldsymbol{r}_1, \boldsymbol{r}_2, \ldots, \boldsymbol{r}_N\}$ is a $3N$-dimensional vector containing all ionic coordinates in the system. It is further decomposed into a series of cyclic paths composed of a finite number M (the Trotter number) of imaginary-time steps (slices) [12] as

$$Z = \int \cdots \int d\boldsymbol{R}d\boldsymbol{R}_1 d\boldsymbol{R}_2 \ldots d\boldsymbol{R}_{M-1} \times \rho(\boldsymbol{R},\boldsymbol{R}_1;\tau)\rho(\boldsymbol{R}_1,\boldsymbol{R}_2;\tau)\ldots\rho(\boldsymbol{R}_{M-1},\boldsymbol{R};\tau). \quad (1)$$

Here, the subscript of $\boldsymbol{R}$ is the numeration of the imaginary-time slice, each of which corresponds to an imaginary-time step of $\tau = \beta/M$. Note that $\boldsymbol{R}_M \equiv \boldsymbol{R}$ for the cyclic path condition. With the so-called quantum-classical isomorphism [52], the quantum system is formally mapped to a classical system, where the potential-energy related part of the classical system's partition function is the same as Eq. (1). This is conceptually equivalent to replacing each quantum particle by a ring polymer consisting of M classical beads (particles) connected with harmonic springs. The PIMD method then samples the microstates of the classical system using a molecular dynamics algorithm, with an appropriately chosen expression for its kinetic energy contribution. More detailed description of the PIMD method can be found elsewhere [39,52].

The PIMD calculation is carried out in canonical (i.e., NVT) ensembles (where V is the volume) using the i-PI code [53], which is linked with the LAMMPS [54] package for the evaluation of ionic interactions. A $2 \times 2 \times 2$ face-centered-cubic (fcc) supercell with periodic boundary conditions is used in the calculation, which consists of $N = 32$ aluminum atoms. The length L of the supercell varies from 7.80 Å to 8.30 Å. T varies in the range from 50 K to 700 K. τ is fixed to be $0.10667k_B^{-1}$ K^{-1} in all simulations in order to maintain a similar precision for all temperatures. This amounts to setting $M = 14$ at $T = 700$ K and $M = 192$ at $T = 50$ K. Each PIMD calculation is conducted for 10^5 steps with a time step of 0.25 fs. In parallel, classical MD calculations at the same temperature are carried out using the LAMMPS package, which are equivalent to PIMD simulations with $M = 1$. The MD calculations are conducted for 2500 ps with a time step of 0.25 fs. The first 10% trajectories in both calculations are used as thermalization, before statistics of physical quantities are taken.

The pressure P of the system is calculated through the virial theorem [55] as

$$P = \frac{1}{3V}\langle 2E_k(\boldsymbol{R}_i,\boldsymbol{R}_{i-1}) + \tilde{V}_{\mathrm{MEAM}}(\boldsymbol{R}_i)\rangle. \quad (2)$$

Here, $\tilde{V}_{\mathrm{MEAM}}$ is the virial contribution from the MEAM potential, and the kinetic energy E_k is calculated as

$$E_k(\boldsymbol{R}_i,\boldsymbol{R}_{i-1}) = \frac{3N}{2\tau} - \frac{\langle(\boldsymbol{R}_i - \boldsymbol{R}_{i-1})^2\rangle}{4\lambda\tau^2}, \quad (3)$$

where the effective mass λ equals $\hbar^2/2m$, with m the mass of an Al ion, and $\hbar$ the Planck constant. The angle brackets $\langle\cdot\rangle$ in Eqs. (2) and (3) represent averages over all M imaginary-time slices and all running (sampling) steps.

To evaluate lattice constant a and bulk modulus B at temperature T, pressures P of several volumes V near the equilibrium volume are first calculated in NVT ensembles, where the temperatures are all fixed at T. The P-V relation $P = P(V)$ is then fitted with a quadratic polynomial. The lattice constant $a(T)$ is determined by the volume $V_{\mathrm{eq}}(T)$ at

the ambient pressure $P = 1.0$ bars from the fitted P-V relation through $a(T) = \sqrt[3]{V_{\rm eq}(T)}/2$. The bulk modulus $B(T)$ can also be determined from the P-V relation as

$$B(T) = -V\left(\frac{\partial P}{\partial V}\right)_T\Big|_{V=V_{\rm eq}(T)}. \tag{4}$$

Higher-order polynomials of $P(V)$ in the fitting process afford similar results with negligible difference from those of quadratic polynomials.

Elastic constant $\mathbb{C}_{ijkl}$ is calculated based on the linear relation

$$\sigma_{ij} = \sum_{k,l} \mathbb{C}_{ijkl}\epsilon_{kl}, \tag{5}$$

where ϵ is the strain tensor, σ is the stress tensor, and indices i, j, k, and l denote the directions along the x, y, z axes in the Cartesian coordinates. In the calculation, a series of finite strains ϵ_{kl} are manually loaded to the supercell, and corresponding stresses σ_{ij} are calculated following the approach described in Refs. [56,57]. The elastic constant $\mathbb{C}_{ijkl}$ is then determined as the slope of the linear fitting function of σ_{ij} with respect to ϵ_{kl}. In a fcc structure, only elastic constants $\mathbb{C}_{xxxx}$, $\mathbb{C}_{xxyy}$, and $\mathbb{C}_{xyxy}$ are used to describe elastic properties of the system, and they are usually denoted as C_{11}, C_{12}, and C_{44}, respectively, following the convention of Voigt. Other elastic constants are either zero or equal to one of these three constants as the result of its symmetry.

III. MEAM POTENTIALS WITH ZERO-POINT FLUCTUATIONS OF IONS

With current MEAM potentials, the PIMD method is generally not able to provide an accurate description to thermal and mechanical properties for metals and alloys at cryogenic temperature, because those potentials were parametrized in compatibility with classical MD methods, which did not take into consideration the influence of the anharmonic ionic interaction to the zero-point fluctuation of ions at low temperature. It is thus desirable to construct new ionic interaction potentials that are compatible with the PIMD method.

As a demonstration, we describe an optimization process for the generation of a revised MEAM potential of Al for accurate PIMD calculation, based on the potential parameters generated for classical MD calculations. The temperature dependency of lattice constant a and bulk modulus B up to room temperature are chosen to be the fitting targets, with precision experimental measurements of a and B [48–50] used as reference data. We note that it is not necessary to start the optimization process from the very beginning with all parameters undetermined. In this way, the computational costs will be tremendous. Instead, it is possible to greatly reduce the computational costs by only optimizing those parameters associated with the zero-point fluctuation of ions. Other parameters can be directly taken from current MEAM potentials for MD methods.

Our trial PIMD simulations show that only two MEAM parameters $\tilde{\alpha}$ and r_e in Pascuet *et al.*'s [34] and Aitken *et al.*'s [35] MEAM potentials are directly associated with a and B. In addition, we find that a very close initial guess to $\tilde{\alpha}$ and r_e can be estimated analytically, which further reduces optimization iterations. Following Alchagirov *et al.*'s [58] approach, zero-point corrections to a at zero temperature, denoted as Δa_0 with subscript 0 representing $T = 0$ K, are estimated as

$$\frac{\Delta a_0}{a_0} = \frac{3}{16}(B_1 - 1)\frac{k_B\Theta_D}{B_0V_0}, \tag{6}$$

where V_0 is the experimental volume at $T = 0$ K, B_0 is bulk modulus at zero temperature, B_1 is the derivative of B_0 with respect to pressure, and Θ_D is the Debye temperature. For bulk modulus B, its zero-point correction ΔB_0 can be similarly estimated as

$$\frac{\Delta B_0}{B_0} = -\frac{3\Delta a_0}{2a_0}(B_1 - 1) - \frac{6\Delta a_0}{a_0}\frac{1}{B_1 - 1}\left(\frac{2}{9} - \frac{1}{3}B_1 - \frac{1}{2}B_0B_2\right), \tag{7}$$

with B_2 the second-order derivative of B_0 with respect to pressure.

The zero-point effect corrected value of a_0, denoted as $\bar{a}_0 = a_0 - \Delta a_0$, is 4.019 Å, and the corrected B_0, denoted as $\bar{B}_0 = B_0 - \Delta B_0$, is 90.6 GPa for Al [21,59]. The parameters r_e and $\tilde{\alpha}$ are then given by $r_e = \bar{a}_0/\sqrt{2}$ and $\tilde{\alpha} = \sqrt{9\bar{B}_0V_0/E_c}$, respectively, where E_c is the cohesive energy of Al. These two corrected parameters, together with other parameters, are then updated through a few optimization iterations to obtain the optimized parameter set. The optimized parameters are determined by minimizing the objective function

$$Q = \sum_i w_i \frac{\left(q_i^{\rm cal} - q_i^{\rm exp}\right)^2}{\left(q_i^{\rm exp}\right)^2}. \tag{8}$$

In Eq. (8), $q_i^{\rm cal}$ refer to the values of fitting targets calculated with the PIMD method, $q_i^{\rm exp}$ stand for the reference data points taken from experiments, and w_i are corresponding weights. The summation is calculated over a series of temperatures below 300 K with equal weights for the two fitting targets a and B. Table I lists the optimized MEAM parameters of Al based on the potential generated by Pascuet *et al.* [34], referred as the M-PR potential hereinafter. Table II displays the optimized parameters based on the MEAM potential of Aitken *et al.* [35], referred as the M-AR potential. Accordingly, the original MEAM potentials of Pascuet *et al.* and Aitken *et al.* will be referred to as the M-P potential and the M-A potential, respectively, for short.

TABLE I. Revised MEAM potential parameters of Al, based on the work of Pascuet *et al.* [34]. The meaning of each parameter is the same as that in Ref. [34].

$\tilde{\alpha}$	$\beta^{(0)}$	$\beta^{(1)}$	$\beta^{(2)}$	$\beta^{(3)}$
5.02977	1.56205	5.39270	5.29601	−1.00047
r_e (Å)	E_c (eV)	A	t_1	t_2
2.839	3.39	1.06859	−1.54917	−1.28508
t_3	d_1	d_2	$C_{\rm min}$	$C_{\rm max}$
10.01041	0.39558	0.09806	1.00769	2.31407

TABLE II. Revised MEAM potential parameters of Al based on the work of Aitken *et al.* [35]. The meaning of each parameter is the same as that in Ref. [35].

$\tilde{\alpha}$	β^0	β^1	β^2	β^3
4.711	3.173	2.342	2.013	2.471
r_e (Å)	E_c (eV)	A	t^1	t^2
2.839	3.427	1.06859	3.285	−0.057
t^3	d_{attrac}	d_{repuls}	C_{min}	C_{max}
5.194	0.063	0.043	0.350	2.539

IV. RESULTS AND DISCUSSION

A. Lattice constant

The lattice constant of Al is displayed in Fig. 1 as a function of T from 0 K to 700 K, where Fig. 1(a) is the results calculated with the M-P potential and the newly revised M-PR potential, and Fig. 1(b) is calculated with the M-A potential and the M-AR potential. The results of the different potentials are distinguished with colors. In both panels, PIMD results are plotted as diamonds, MD results are displayed as circles, and experimental data are displayed as solid curves.

It shows that PIMD and MD results start to deviate from each other at a threshold temperature between 200 K and 250 K, which is roughly half of the Debye temperature of 428 K. Above that temperature, both PIMD and MD lattice constants display a linear dependence with respect to temperature. However, when temperature is lower than the threshold temperature, the PIMD lattice constant gradually converges to a constant value, while the MD lattice constant keeps a linear temperature-dependent relation. Since the deviation is regarded as a typical feature of the zero-point effect of ionic motion [60,61], this high threshold temperature, which is between 200 K and 250 K, suggests the importance to take quantum effects into consideration for metal and alloy.

TABLE III. PIMD results of lattice constant a at $T = 50$ K, 300 K, and 700 K. The difference $\Delta a = a - a_{\text{Expt}}$ with respect to experimental value (Expt.) [48] and corresponding percentage difference $\Delta a/a_{\text{Expt}}$ are listed in the last two columns. Numbers in parentheses are numerical uncertainties of the last digit.

T (K)	Potential	a (Å)	Δa (Å)	$\Delta a/a_{\text{Expt}}$ (%)
50	M-P	4.0682(1)	0.0365	0.90
	M-A	4.0606(2)	0.0289	0.72
	M-PR	4.0329(2)	0.0011	0.03
	M-AR	4.0330(1)	0.0012	0.03
	(Expt.)	4.0318		
300	M-P	4.0844(7)	0.0360	0.89
	M-A	4.0746(4)	0.0262	0.65
	M-PR	4.0474(7)	−0.0010	−0.02
	M-AR	4.0467(5)	−0.0017	−0.04
	(Expt.)	4.0484		
700	M-P	4.1374(2)	0.0451	1.10
	M-A	4.1089(5)	0.0166	0.41
	M-PR	4.0952(9)	0.0029	0.07
	M-AR	4.0796(9)	−0.0127	−0.31
	(Expt.)	4.0923		

When compared with experimental measurements, displayed as solid curves in the figure, Fig. 1 shows that the two original MEAM potentials generally overestimate the lattice constant for both PIMD and MD calculations. The overestimation is about 1% at room temperature and above. At low temperature, the overestimation by the MD calculation is slightly reduced as a result of not including zero-point fluctuations. This overestimation shows the necessity of a new Al potential for an accurate description of thermal properties at low temperature.

With the revised MEAM potentials, of which the parameters are listed in Tables I and II, the overestimation is essentially reduced. Table III provides a detailed comparison for the improvement. It shows that with the correction of zero-point fluctuations, the PIMD lattice constant with both

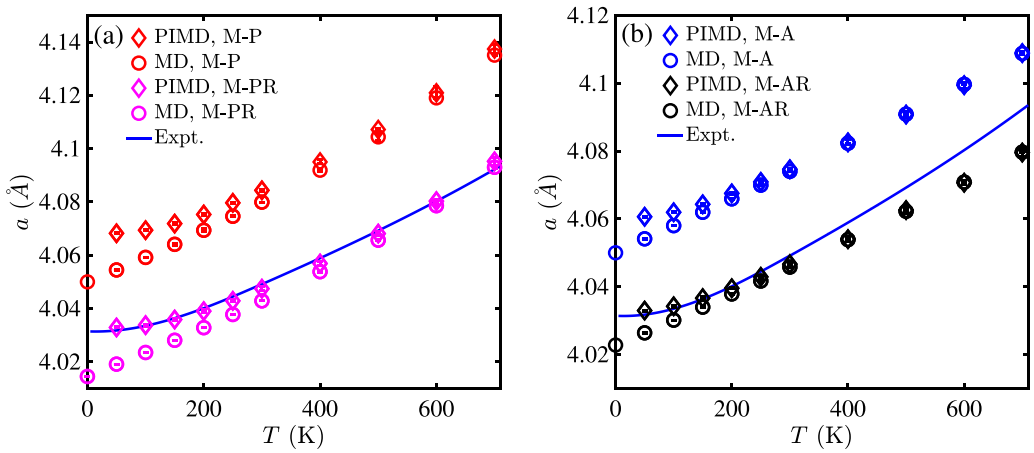

FIG. 1. Lattice constant a of Al as a function of T, calculated by the PIMD and MD methods. Experimental measurements taken from Ref. [48] are also presented for the comparison purpose. (a) PIMD and MD results calculated with the M-P and the M-PR potentials. (b) PIMD and MD results calculated with the M-A and the M-AR potentials.

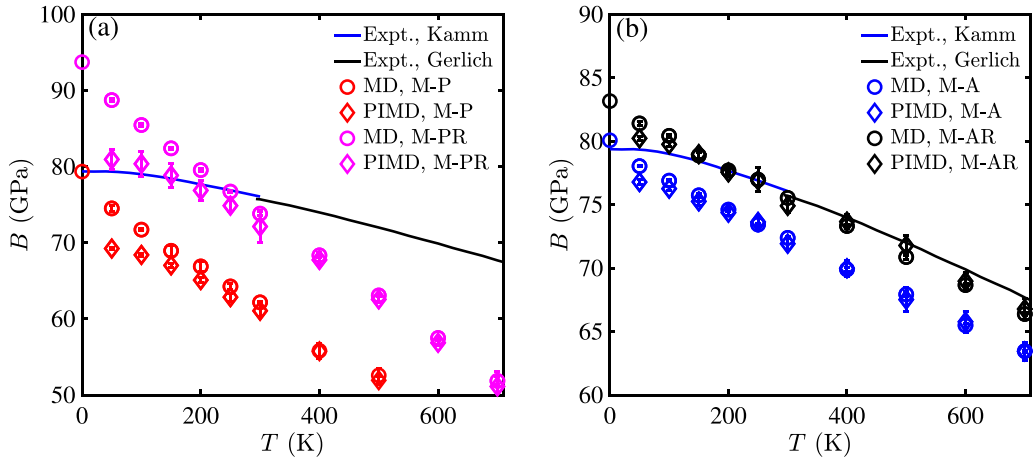

FIG. 2. Bulk modulus B of Al as a function of T, calculated with the PIMD and MD methods. Experimental results of Kamm *et al.* [49] and Gerlich *et al.* [50] are also presented with blue and black curves, respectively, for the comparison purpose. (a) PIMD and MD results calculated with the M-P and the M-PR potentials. (b) PIMD and MD results calculated with the M-A and the M-AR potentials.

revised potentials has arrived at such an accuracy that its deviation with respect to experimental data is less than 0.05% around room temperature and below. Moreover, in the temperature range from 300 K to 700 K, the M-PR potential has an excellent performance. The largest deviation in lattice constant is about 0.07% at 700 K. The M-AR potential slightly underestimates the lattice constant in this temperature range. However, compared with the original M-A potential, the largest deviation is no more than 0.31%, which is still a very accurate result.

B. Bulk modulus

In Fig. 2, the isothermal bulk modulus B at atmospheric pressure (1.0 bars) is presented as a function of temperature up to 700 K. The zero-point effect appears at a similar threshold temperature as that of the lattice constant, as can be seen from the differences between PIMD and MD calculations. The similar threshold temperature for the arising of the zero-point effect in both thermal properties, i.e., the lattice constant and bulk modulus, may not be an accident. In a rough picture, assuming that anharmonic interaction is neglected, the motion of ions can be viewed as the superposition of a series of simple oscillation motions (i.e., phonon modes). For each oscillation mode, the probability density $\tilde{\rho}(q)$ with respect to its general coordinate q is $\tilde{\rho}(q) \propto \exp[-q^2(\omega/\hbar)\tanh(\hbar\omega/2k_BT)]$ [17], where ω is the frequency of the mode, and $\hbar$ is the Planck constant. $\tilde{\rho}(q)$ approaches the classical distribution, proportional to $\exp(-q^2\omega^2/2k_BT)$, as the tanh function goes to zero, and approaches the quantum distribution proportional to $\exp(-q^2\omega/\hbar)$, i.e., the distribution dominant by the zero-point fluctuation, as the tanh function goes to 1. It is reasonable to use the inflection point of the tanh function as the starting threshold of the zero-point effect, which corresponds to a temperature $T_{th} = \hbar\omega/2k_B$. In a solid, the Debye temperature Θ_D is related to the frequency of the highest-energy mode by $\Theta_D = \hbar\omega_{\max}/k_B$. It is thus not surprising that one observes a threshold temperature about half of the Debye temperature. As a rule of thumb, one may consider using a fraction of the Debye temperature, instead of the temperature at which the thermal wavelength is comparable with the distance between ions, as an indication of the appearance of zero-point effect in a solid.

Figure 2 also shows that original MEAM potentials have a significant underestimation to bulk modulus for all temperatures under consideration, when compared with experimental data. With the revised potentials, however, the results are much improved. Table IV provides a quantitative comparison of PIMD predictions of the bulk modulus for all four potentials, at 50 K, 300 K, and 700 K. At $T = 50$ K, the bulk modulus calculated by the M-P potential has an underestimation of 12.73%, and the M-A potential underestimates the bulk modulus by 3.23%. With the revised potentials, the deviation is much reduced to 2.01% for the M-PR potential, and 1.12% for the M-AR potential. Note that both revised potentials slightly overestimate the bulk modulus while the

TABLE IV. PIMD results of bulk modulus B at $T = 50$ K, 300 K, and 700 K. The difference $\Delta B = B - B_{\text{Expt}}$ with respect to experimental value (Expt.) [49,50] and corresponding relative error $\Delta B/B_{\text{Expt}}$ are listed in the last two columns. Numbers in parentheses are numerical uncertainties of the last digit.

T (K)	Potential	B (GPa)	ΔB (GPa)	$\Delta B/B_{\text{Expt}}$ (%)
50	M-P	69.3(8)	−10.1	−12.73
	M-A	76.8(2)	−2.6	−3.23
	M-PR	81.0(9)	1.6	2.02
	M-AR	80.2(2)	0.8	1.12
	(Expt.)	79.4		
300	M-P	61.1(8)	−14.6	−19.34
	M-A	71.9(4)	−3.8	−4.72
	M-PR	72.1(9)	−3.6	−5.18
	M-AR	74.9(6)	−0.8	−1.04
	(Expt.)	75.7		
700	M-P	40.5(8)	−27.2	−40.17
	M-A	63.4(7)	−4.3	−6.28
	M-PR	51.1(9)	−16.6	−24.46
	M-AR	66.8(8)	−0.9	−1.34
	(Expt.)	67.7		

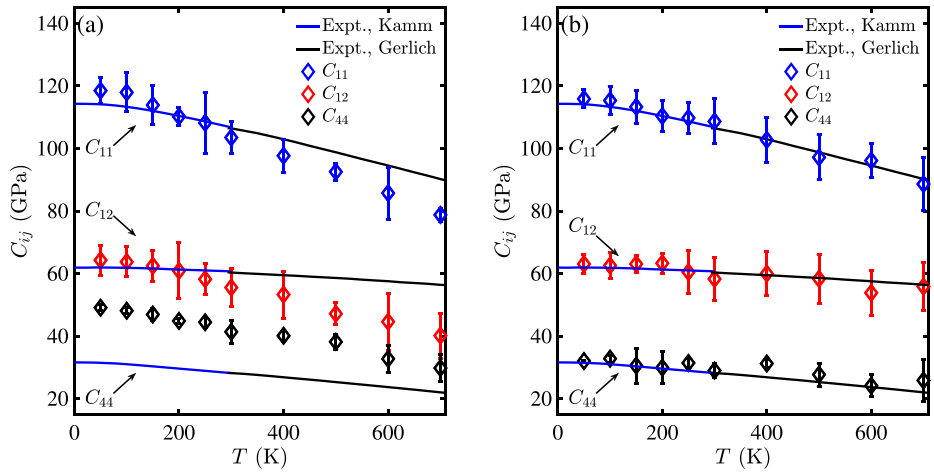

FIG. 3. Temperature dependencies of elastic constants for aluminum, calculated with the PIMD method. The diamonds in blue, red, and black stand for the results of C_{11}, C_{12}, and C_{44}, respectively. Experimental results of Kamm *et al.* [49] and Gerlich *et al.* [50] are also presented with blue and black solid curves, respectively, for comparison purposes. (a) Results calculated with the M-PR potential. (b) Results calculated with the M-AR potential.

original potentials underestimate it. At $T = 300$ K, the deviation of the revised M-PR potential is reduced to 5.18% from the deviation of 19.34% of the original M-P potential, and the error of the M-AR potential is 1.04%, much smaller than the error 4.72% of the M-A potential.

As displayed in Fig. 2, the two revised potentials have very different performances at T above 300 K. For the M-PR potential, the PIMD prediction to bulk modulus has an increasing deviation. The largest deviation of −24.46% appears at $T = 700$ K. However, the M-AR potential maintains a good performance at T above 300 K. The PIMD results keep a small error about 1% for all temperatures from 300 K to 700 K. The largest deviation of 1.34% takes place at $T = 700$ K. The good performance of both revised potentials at temperatures below 300 K is within the anticipation, since the potentials are optimized in this temperature range. The good performance of the M-AR potential may suggest it having a much larger application range not confined at low temperature.

C. Elastic constants

Figures 3(a) and 3(b) display the PIMD calculation of elastic constants C_{11}, C_{12}, and C_{44} with the two revised MEAM potentials. The elastic constant C_{11}, which describes the stress response in the direction parallel to the stretch, shows a similar temperature dependency as that of lattice constant and bulk modulus. At low temperature, C_{11} converges to a constant value as the result of the quantum zero-point fluctuation of ions, which is similar to the trend displayed in the calculations of a and B. C_{12} describes the perpendicular stress response to a stretch, and C_{44} is for the response of shearing motion. Both C_{12} and C_{44} have a different temperature-dependent relation from that of C_{11}. As can be observed from experimental measurements, they are nearly independent of temperature for all T below 700 K, which implies that the interplay between the quantum effects and the ionic potential has a minor influence on them.

The two revised MEAM potentials perform quite differently in the calculation of elastic constants. As displayed in Fig. 3(b), the M-AR potential results show excellent agreement with experimental measurements for all temperatures below 700 K. Quantitatively, the maximal differences for C_{11}, C_{12}, and C_{44} are 3.98%, 6.48%, and 17.24%, respectively. The maximal difference will further decreases to 2.16%, 4.11%, and 8.19%, respectively, if the potential is applied to a temperature below 300 K, i.e., below the room temperature. The C_{11} and C_{12} calculated with the M-PR potential agree well with the experimental data at temperatures below 300 K. But they are significantly underestimated when T is higher. This is consistent with the trend revealed in the calculation of B shown in Fig. 2(a), since $B = (C_{11} + 2C_{12})/3$. The relation between bulk modulus and elastic constants also shows that the temperature dependency is actually contributed by C_{11}, considering C_{12} is nearly temperature independent. The C_{44}'s calculated with the M-PR potential are generally about 30% to 50% higher than the experimental results for all temperatures below 700 K, showing that the shearing-related properties predicted by the M-PR potential will be less accurate than those predicted with the M-AR potential.

V. CONCLUSION

In summary, we show that an accurate description of thermal and mechanical properties of Al at low temperature can be achieved by the PIMD method together with particularly revised empirical MEAM potentials, as long as the interplay between the highly anharmonic ionic interaction and zero-point fluctuation of ions is carefully taken into consideration. The revision procedure of the MEAM potential also provides a possible option to further improve the

accuracy of low-temperature ionic potentials generated based on quantum-mechanical calculations by taking the correction from experimental measurements into consideration.

ACKNOWLEDGMENT

This work is supported by the Science Challenging Project (Grant No. TZ2016001).

[1] G. J. Snyder and E. S. Toberer, Nat. Mater. **7**, 105 (2008).
[2] I. Levchenko, S. Xu, G. Teel, D. Mariotti, M. L. R. Walker, and M. Keidar, Nat. Commun. **9**, 879 (2018).
[3] I. Levchenko, K. Bazaka, T. Belmonte, M. Keidar, and S. Xu, Adv. Mater. **30**, 1802201 (2018).
[4] H. Abu-Shawareb, R. Acree, P. Adams, J. Adams, B. Addis, R. Aden, P. Adrian, B. B. Afeyan, M. Aggleton, L. Aghaian, A. Aguirre, D. Aikens, J. Akre, F. Albert, M. Albrecht, B. J. Albright, J. Albritton, J. Alcala, C. Alday, D. A. Alessi *et al.*, Phys. Rev. Lett. **129**, 075001 (2022).
[5] A. B. Zylstra, A. L. Kritcher, O. A. Hurricane, D. A. Callahan, J. E. Ralph, D. T. Casey, A. Pak, O. L. Landen, B. Bachmann, K. L. Baker, L. Berzak Hopkins, S. D. Bhandarkar, J. Biener, R. M. Bionta, N. W. Birge, T. Braun, T. M. Briggs, P. M. Celliers, H. Chen, C. Choate *et al.*, Phys. Rev. E **106**, 025202 (2022).
[6] T. Debnath, D. Sarker, H. Huang, Z.-K. Han, A. Dey, L. Polavarapu, S. V. Levchenko, and J. Feldmann, Nat. Commun. **12**, 2629 (2021).
[7] S. Chen, D. Coleman, D. L. Abernathy, A. Banerjee, L. L. Daemen, L. Mangolini, and C. W. Li, Phys. Rev. Mater. **4**, 056001 (2020).
[8] L. L. Araujo, P. Kluth, G. de M. Azevedo, and M. C. Ridgway, Phys. Rev. B **74**, 184102 (2006).
[9] L. L. Araujo, R. Giulian, D. J. Sprouster, C. S. Schnohr, D. J. Llewellyn, P. Kluth, D. J. Cookson, G. J. Foran, and M. C. Ridgway, Phys. Rev. B **78**, 094112 (2008).
[10] T. Comaschi, A. Balerna, and S. Mobilio, Phys. Rev. B **77**, 075432 (2008).
[11] S. H. Lohaus, M. B. Johnson, P. F. Ahnn, C. N. Saunders, H. L. Smith, M. A. White, and B. Fultz, Phys. Rev. Mater. **4**, 086002 (2020).
[12] R. P. Feynman and A. R. Hibbs, *Quantum Mechanics and Path Integrals* (McGraw-Hill, New York, 1965).
[13] B. J. Alder and T. E. Wainwright, J. Chem. Phys. **31**, 459 (1959).
[14] M. Ben-Nun and R. D. Levine, J. Chem. Phys. **105**, 8136 (1996).
[15] L. Boeri, E. Cappelluti, and L. Pietronero, Phys. Rev. B **71**, 012501 (2005).
[16] H. Mishra and S. Bhattacharya, Phys. Rev. B **99**, 165201 (2019).
[17] R. P. Feynman, *Statistical Mechanics* (Benjamin, New York, 1972).
[18] J. Sun, A. Ruzsinszky, and J. P. Perdew, Phys. Rev. Lett. **115**, 036402 (2015).
[19] J. Sun, R. C. Remsing, Y. Zhang, Z. Sun, A. Ruzsinszky, H. Peng, Z. Yang, A. Paul, U. Waghmare, X. Wu, M. L. Klein, and J. P. Perdew, Nat. Chem. **8**, 831 (2016).
[20] K. Sharkas, K. Wagle, B. Santra, S. Akter, R. R. Zope, T. Baruah, K. A. Jackson, J. P. Perdew, and J. E. Peralta, Proc. Natl. Acad. Sci. USA **117**, 11283 (2020).
[21] P. Haas, F. Tran, and P. Blaha, Phys. Rev. B **79**, 085104 (2009).
[22] J. P. Perdew and K. Schmidt, AIP Conf. Proc. **577**, 1 (2001).
[23] M. S. Daw and M. I. Baskes, Phys. Rev. Lett. **50**, 1285 (1983).
[24] M. S. Daw and M. I. Baskes, Phys. Rev. B **29**, 6443 (1984).
[25] S. M. Foiles, M. I. Baskes, and M. S. Daw, Phys. Rev. B **33**, 7983 (1986).
[26] K. W. Jacobsen, J. K. Norskov, and M. J. Puska, Phys. Rev. B **35**, 7423 (1987).
[27] J. Mei and J. W. Davenport, Phys. Rev. B **46**, 21 (1992).
[28] Y. Mishin, D. Farkas, M. J. Mehl, and D. A. Papaconstantopoulos, Phys. Rev. B **59**, 3393 (1999).
[29] H. W. Sheng, M. J. Kramer, A. Cadien, T. Fujita, and M. W. Chen, Phys. Rev. B **83**, 134118 (2011).
[30] M. I. Baskes, Phys. Rev. B **46**, 2727 (1992).
[31] B. J. Lee and M. I. Baskes, Phys. Rev. B **62**, 8564 (2000).
[32] B. J. Lee, M. I. Baskes, H. Kim, and Y. K. Cho, Phys. Rev. B **64**, 184102 (2001).
[33] B. J. Lee, J. H. Shim, and M. I. Baskes, Phys. Rev. B **68**, 144112 (2003).
[34] M. I. Pascuet and J. R. Fernández, J. Nucl. Mater. **467**, 229 (2015).
[35] Z. H. Aitken, V. Sorkin, Z. G. Yu, S. Chen, Z. X. Wu, and Y. W. Zhang, Phys. Rev. B **103**, 094116 (2021).
[36] J. Tersoff, Phys. Rev. Lett. **61**, 2879 (1988).
[37] J. Tersoff, Phys. Rev. B **44**, 12039 (1991).
[38] J. Tersoff, Phys. Rev. B **49**, 16349 (1994).
[39] D. Marx and M. Parrinello, J. Chem. Phys. **104**, 4077 (1996).
[40] M. Chen, E. Ma, K. J. Hemker, H. Sheng, Y. Wang, and X. Cheng, Science **300**, 1275 (2003).
[41] V. Yamakov, D. Wolf, S. R. Phillpot, A. K. Mukherjee, and H. Gleiter, Nat. Mater. **1**, 45 (2002).
[42] V. Yamakov, D. Wolf, S. R. Phillpot, and H. Gleiter, Acta Mater. **50**, 5005 (2002).
[43] J. Rajagopalan, J. H. Han, and M. T. Saif, Science **315**, 1831 (2007).
[44] Y. Shi and I. Szlufarska, J. Mater. Sci. **56**, 14587 (2021).
[45] J. Hohl, P. Kumar, M. Misra, P. Menezes, and L. T. Mushongera, J. Mater. Sci. **56**, 14611 (2021).
[46] G. H. Balbus, J. Kappacher, D. J. Sprouster, F. L. Wang, J. Shin, Y. M. Eggeler, T. J. Rupert, J. R. Trelewicz, D. Kiener, V. Maier-Kiener, and D. S. Gianola, Acta Mater. **215**, 116973 (2021).
[47] S. V. Razorenov, Matter Radiat. Extremes **3**, 145 (2018).
[48] V. S. Touloukian, R. K. Kirby, R. E. Taylor, and P. D. Desai, *Thermal Expansion: Metallic Elements and Alloys, Thermophysical Prosperities of Matter* (Plenum, New York, 1975), Vol. 12.
[49] G. N. Kamm and G. A. Alers, J. Appl. Phys. **35**, 327 (1964).
[50] D. Gerlich and E. S. Fisher, J. Phys. Chem. Solids **30**, 1197 (1969).
[51] J. L. Tallon and A. Wolfenden, J. Phys. Chem. Solids **40**, 831 (1979).
[52] C. P. Herrero and R. Ramírez, J. Phys.: Condens. Matter **26**, 233201 (2014).
[53] M. Ceriotti, J. More, and D. E. Manolopoulos, Comput. Phys. Commun. **185**, 1019 (2014).

[54] S. Plimpton, J. Comput. Phys. **117**, 1 (1995).
[55] D. M. Ceperley, Rev. Mod. Phys. **67**, 279 (1995).
[56] L. A. P. Ardila, S. A. Vitiello, and M. de Koning, Phys. Rev. B **84**, 094119 (2011).
[57] B. G. A. Brito, G.-Q. Hai, and L. Cândido, Comput. Mater. Sci. **173**, 109387 (2020).
[58] A. B. Alchagirov, J. P. Perdew, J. C. Boettger, R. C. Albers, and C. Fiolhais, Phys. Rev. B **63**, 224115 (2001).
[59] V. N. Staroverov, G. E. Scuseria, J. Tao, and J. P. Perdew, Phys. Rev. B **69**, 075102 (2004).
[60] C. P. Herrero, Solid State Commun. **110**, 243 (1999).
[61] C. P. Herrero and R. Ramírez, Phys. Rev. B **63**, 024103 (2000).